# Temperature-dependent coherent oscillation in photorefractive relaxor strontium barium niobate

**M. Goulkov and O. Fedorenko**

*Institute of Physics, Science Avenue 46, 03650, Kiev-39, Ukraine*

**L. Ivleva**

*Institute of General Physics, Moscow, Russia*

**Th. Woike**

*Institute of Mineralogy, University of Cologne, Germany*

**T. Granzow**

*Institute of Mineralogy, University of Cologne, Germany and*
*Institute of Materials Science, Darmstadt University of Technology, Germany*

**M. Imlau and M. Wöhlecke**

*Department of Physics, University Osnabrück, Germany*

Received November 10, 2004; revised manuscript received February 23, 2005; accepted February 24, 2005

A temperature study of a photorefractive coherent oscillation in a ring-loop resonator with the relaxor ferroelectric $Sr_{0.61}Ba_{0.39}Nb_2O_6$:Ce as a nonlinear element is presented. It is shown that the oscillation intensity as well as the oscillation onset time strongly depend on the crystal temperature. Strong influence of a resonator loop angle on the temperature dependence of coherent oscillation is reported and discussed via the dispersion of thermal spatial disorder and thermal decay versus various scales in the polar structure. Optimization of the output of a photorefractive oscillator via thermal tuning of material parameters of the crystal is shown.

*OCIS codes:* 160.5320, 160.2260, 190.5330.

## 1. INTRODUCTION

The photorefractive effect is a characteristic nonlinear optic phenomenon well utilized for the recording of volume phase gratings in many ferroelectric crystals.[1] The grating recording can be sequenced to (i) a conversion of the interference pattern of two coherent light waves into a space-charge field induced by photoinduced electric carriers and (ii) a spatial modulation of the refractive index by the field via the linear electro-optic effect. Mutual diffraction of the recording waves on the refractive index grating causes a change of the amplitudes and–or phases of the waves that in turn modifies the recording process. This real-time feedback is a favorable condition for nonlinear wave mixing that makes photorefractive ferroelectrics very suitable for different applications. One of the most prominent manifestations of the wave mixing is coherent oscillation in optical resonators with a photorefractive nonlinear medium.[2] An oscillator emits an optical signal that is phase conjugated to the incident pump beam as a result of the selective amplification of noisy photorefractive gratings via four-wave mixing (4WM) processes. The efficiency of coherent oscillation depends on the particular geometry of the wave mixing and on material parameters of the crystal. Optimization and deliberate tuning of the performance of photorefractive oscillators are important for their applications in optical image transmission and computing systems, self-adjustable interferometers, logical and bistable elements, and optical nonlinear associative memory.[3]

The strong correlation between photorefractive and ferroelectric properties allows us to control photorefraction-related phenomena in ferroelectrics via a change of the electric polarization $P_s$. In turn, the study of the photorefractive response can give an important insight into the polar structure of a ferroelectric and particularly allows us to study its temperature-dependent decay due to the ferroelectric-paraelectric phase transition. Recently, first attempts were made to detect the temperature of the phase transition and ferroelectric hysteresis by means of the photorefractive light-induced scattering (beam fanning) in $Sr_{0.61}Ba_{0.39}Nb_2O_6$ (strontium barium niobate) doped with Cerium (SBN:Ce).[4,5] SBN undergoes the phase transition close to room temperature, showing strong relaxor behavior; the polar structure does not van-

ish abruptly at a particular temperature but gradually decays in a wide temperature interval. The broad temperature distribution of the decay of local polar structures of different size $\Lambda_d$ is suggested as one of the reasons for such smearing of the phase transition.[6] It is clear then that the photorefractive response in SBN should exhibit a maximum when approaching the phase transition and then decline at higher temperatures. The strong relaxor properties of SBN allow some remanent photorefractive recording, even in the paraelectric phase. The high spatial selectivity of a photorefractive resonator suggests that the oscillation process is very susceptible to state changes of a polar structure with a certain size of $\Lambda_d$, which correlates with the spatial grating period defined by the corresponding 4WM geometry. Also, because of its pronounced threshold behavior, the dynamics of coherent oscillation is expected to be an especially sensitive tool in measuring changes in the polar structure induced by heating.

In this paper we report on the study of coherent oscillation in SBN:Ce in a ring-loop resonator in a wide temperature interval encompassing the phase transition. The temperature dependence of the dynamics and the steady state of coherent oscillation measured at different loop angles of the resonator are discussed and interpreted with respect to the relaxor properties of SBN. We show that this study can give insight into the thermal spatial disorder and the posterior thermal decay of the polar structure in the crystal bulk. The high selectivity of the ring-loop oscillator enables us to distinctly reveal the strong difference of the disorder–decay processes for ferroelectric domains of different size $\Lambda_d$. It is shown that the performance of the ring-loop oscillator can be optimized by temperature tuning.

## 2. BASIC MODEL ASSUMPTIONS

A photorefractive ring-loop oscillator with four waves mixed in a SBN crystal is shown in Fig. 1. The laser beam pumps the crystal as wave 2 and then is reflected by the mirrors Mr1 and Mr2 back to the crystal as wave 4. Noisy waves 3 and 1 are counterpropagating to waves 4 and 2, respectively. If the length of the resonator cavity $L$ is larger than the laser coherence length $l_c$, only the grating $\mathbf{K}_g=\mathbf{k}_2-\mathbf{k}_3=\mathbf{k}_4-\mathbf{k}_1$ is recorded by pairs of mutually coherent waves 3–2 and 1–4. The grating period $\Lambda_g=2\pi/|\mathbf{K}_g|=\frac{1}{2}\lambda/\sin(\theta_{\text{loop}}/2)$ is defined by the geometry of the ring-loop resonator. In SBN, characterized by a pure nonlocal photorefractive response, wave mixing on the grating $\mathbf{K}_g$ results in an amplification of waves 3 and 1 at the expense of waves 2 and 4 if the crystal polar **c** axis is aligned as shown in Fig. 1. The neutral density (ND) filter with tunable transmission in the loop cavity controls optical losses.

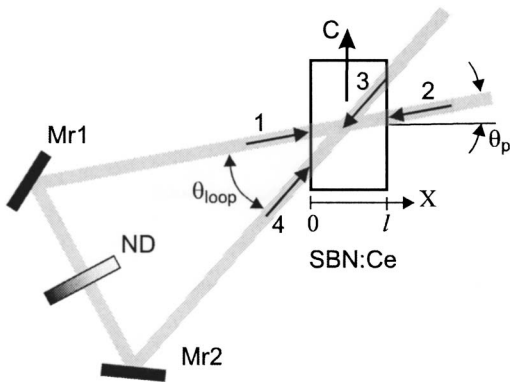


Fig. 1. The ring-loop resonator is built with a crystal of SBN:Ce and two plane mirrors Mr1 and Mr2. The pump beam 2 ($\lambda=488$ nm) impinges upon the crystal at the angle $\theta_p=1°$. The resonator cavity angle was adjusted to three different values $\theta_{\text{loop}}$: 27°, 14.5°, and 4.5°.

An amplification rate of the photorefractive crystal in a particular interaction geometry is defined by the coupling strength $(\Gamma l)_o$, which is the product of the interaction length $l$ and the nonlinear coupling coefficient $\Gamma_o=4\pi\lambda^{-1}(\Delta n)_o$, where $(\Delta n)_o$, is the amplitude of the grating $\mathbf{K}_g$. The length $l$ can be roughly estimated as the crystal thickness. Below the oscillation threshold the coupling strength rises in time to its saturation value $(\Gamma l)_o$ as

$$(\Gamma l)(t)=(\Gamma l)_o[1-\exp(-t/\tau_{\text{di}})], \tag{1}$$

where $\tau_{\text{di}}=\epsilon\epsilon_o/\sigma$ is the dielectric relaxation time dependent on the dielectric permittivity $\epsilon$, the dielectric constant $\epsilon_o$, and the conductivity $\sigma$. Coherent oscillation emerges when the coupling strength $(\Gamma l)(t)$ reaches the threshold value[2]:

$$(\Gamma l)_{\text{th}}=-2\frac{M+1}{M-1}\ln\frac{M+1}{2M}, \tag{2}$$

where $M=M_{\text{ND}}R_1R_2(1-R_F)^2$ is the total transmission coefficient of the loop cavity, depending on the reflection coefficients of the two mirrors $R_1$ and $R_2$, the Fresnel losses $R_F$ on the crystal surfaces, and the transmission coefficient $M_{\text{ND}}$ of the ND filter. According to Eqs. (1) and (2) the oscillation starts at the characteristic onset time[7]:

$$t_{\text{on}}=-\tau_{\text{di}}\ln\left[1+\frac{2(M+1)}{(\Gamma l)_o(M-1)}\ln\frac{M+1}{2M}\right], \tag{3}$$

which is the delay time between the beginning of the illumination of the crystal and the first emergence of a collimated oscillator output. It should be noted that simple exponential dynamics according to Eq. (1) are valid only with the assumption of an interference pattern with low, uniform contrast throughout the crystal thickness. These conditions are fulfilled only below and close to the oscillation threshold ($t\leqslant t_{\text{on}}$), where the signal $I_1$ has the same order of magnitude as the coherent noise, that is, much lower than the pump-beam intensity $I_2$. For $t\gg t_{\text{on}}$, the grating $\mathbf{K}_g$ becomes stronger, and further dynamics of the coherent oscillation, corresponding to the approach of the steady state, are influenced by the beam-coupling process.[8]

According to Eqs. (2) and (3), the threshold coupling strength $(\Gamma l)_{\text{th}}$ and the onset time $t_{\text{on}}$ nonlinearly depend on the loop transmission coefficient and increase with decreasing $M$. If the transmission is reduced so that the loop threshold $(\Gamma l)_{\text{th}}$ reaches the amplification limit $(\Gamma l)_{\text{th}}=(\Gamma l)_o$, $t_{\text{on}}$ approaches infinity. The corresponding value of the transmission coefficient will be referred to as $M_{\text{th}}$. A further decrease of the transmission ($M<M_{\text{th}}$) results in

no oscillation at all. Therefore, to achieve a small onset time and a high output signal, the condition $(\Gamma l)_{\mathrm{th}} \ll (\Gamma l)_o$ must be fulfilled. Lowering of the threshold $(\Gamma l)_{\mathrm{th}}$ is possible via the reduction of optical losses of the cavity, e.g., by use of mirrors with a high reflectivity and antireflective coating on the crystal surfaces. The increase of $(\Gamma l)_o$ requires a strengthening of the grating $\mathbf{K}_g$.

The photorefractive grating $\mathbf{K}_g$ is the result of a spatial modulation of the index of refraction by the space-charge field via the linear electrooptic effect. In SBN, the space-charge field is induced by the diffusion-driven redistribution of photoexcited electrons in the crystal bulk. Therefore the grating amplitude $(\Delta n)_o$ is defined by the amplitude of the effective diffusion field $E_{\mathrm{dif}} = k_B T e^{-1} K_g [1 + (K_g/K_D)^2]^{-1}$, where $T$ is the crystal temperature, $e$ is the elementary charge, $K_D = (e^2 N_{\mathrm{eff}}/\epsilon\epsilon_o k_B T)^{1/2}$ is the Debye screening length, and $N_{\mathrm{eff}}$ is the effective trap density. The dependence of the diffusion charge transport on $\mathbf{K}_g$ leads to a dependence of the coupling strength $(\Gamma l)_o$ and the oscillation intensity $I_1(l)$ on the loop angle $\theta_{\mathrm{loop}}$. On the other hand, the amplitude $(\Delta n)_o$ is dependent on the effective linear electro-optic coefficient $r_{\mathrm{eff}}$, which is governed by the electric polarization $P_s$ and dielectric permittivity $\epsilon$[9]:

$$r_{\mathrm{eff}} = 2 g P_s \epsilon \epsilon_o, \tag{4}$$

where $g$ is the quadratic electro-optic coefficient. Thus the output of the ring-loop resonator can be controlled by manipulating the polar structure of the crystal. SBN is actually not a single-domain crystal but instead consists of a multitude of domains of different sizes $\Lambda_d$ that, however, can be aligned in one direction by applying an external field.[10] A ferroelectric with a well-ordered polar structure provides a large value $P_s$ and, respectively, a high coefficient $\Gamma_o$. If such an electrically poled SBN crystal is then gradually heated to the phase-transition temperature, the thermal decay of the polar structure is anticipated by the thermally induced spatial disorder of ferroelectric domains at much lower temperatures.

The relaxor properties combined with a relatively low temperature of the phase transition have a remarkable effect on the temperature dependence of the photorefractive response and coherent oscillation in SBN. Because of strong "smearing" of the phase transition, the maxima of $\epsilon(T)$ and $r_{\mathrm{eff}}(T)$ are largely broadened, and the coupling coefficient $\Gamma_o$ exhibits strong changes over a wide temperature range near room temperature. Therefore coherent oscillation will exhibit two different stages: (1) enhancement near to the phase transition and (2) suppression after the thermal decay of the polar structure begins. A particularly pronounced dependence on any (even rather small) changes in the polar structure is expected for the oscillation threshold because of its heavily nonlinear dependence on $\Gamma_o$. Moreover, the "noisy" origin of wave 3 and the impact of the domain arrangement on the coherent noise in SBN should provide an additional correlation between the oscillation signal and the state of the polar structure. According to the model of seed scattering in SBN,[5] scattering centers are incorporated in the polar structure and also make up spatially ordered structures in the poled sample. The most efficient scattering on structures associated with domains of the size $\Lambda_d$ occurs at the angle $\theta_s$:

$$\theta_s = 2 \arcsin(\lambda/2\Lambda_d). \tag{5}$$

4WM results in a selective amplification of coherent noise propagating at the angle $\theta_s = \theta_{\mathrm{loop}}$. In this case, the spatial period $\Lambda_g$ of the grating $\mathbf{K}_g$ is correlated with only one particular domain size $\Lambda_d$. This can be used to study the temperature behavior of the decay of domains of one particular size defined by $\theta_{\mathrm{loop}}$.

## 3. EXPERIMENTAL DETAILS AND RESULTS

All measurements were performed with a crystal of $Sr_{0.61}Ba_{0.39}Nb_2O_6$ grown by the modified Stepanov technique[11] and doped with 0.01 wt% $CeO_2$. The phase-transition temperature estimated from the temperature dependence of the dielectric response is 78 °C. The crystal was cut into a rectangular parallelepiped with dimensions $X \times Y \times Z = 8.2 \times 2.7 \times 9.6$ mm$^3$, and electrically poled along the longest side parallel to the crystallographic **c** axis. The crystal mounted on a Peltier element and two highly reflecting mirrors Mr1 and Mr2 ($R_1 = R_2 = 0.99$) made a ring-loop cavity. The temperature of the crystal was varied from 5 °C to 80 °C. The crystal is illuminated by coherent light after the desired temperature is stabilized. The beam of an $Ar^+$-ion laser ($\lambda = 488$ nm, $d_{\mathrm{FWHM}} = 0.8$ mm) impinged on the sample at a pump angle $\theta_p = 1°$ with respect to the surface normal, labeled X; see Fig. 1. A moderate pump intensity of $I_p = I_2(l) = 1.3$ W/cm$^2$ was used. The extraordinary polarization of the beam involves the largest linear electro-optic coefficient $r_{33}$ in the photorefractive recording. To avoid the recording of reflection gratings by the pump waves 2 and 4 and by the seed waves 3 and 1, we chose the resonator length $L = 110$ cm much larger than the laser coherence length $l_c = 6$ cm. The Fresnel loss on the crystal surface was estimated to be $R_F = 0.15$. The coherent oscillation intensity $I_1(l)$ was measured in real time and normalized to the input intensity of the pump beam $I_2(l)$. The cavity transmission was varied by changing $M_{\mathrm{ND}}$. Measurements were carried out for three different loop angles $\theta_{\mathrm{loop}} = 4.5°$, 14.5°, and 27°.

Typical oscillation dynamics at different temperatures for the three angles are presented in Fig. 2. The proper curve order is traced via the dotted line with arrows in the direction of temperature increase. It shows that the onset time $t_{\mathrm{on}}$ does not change monotonically with temperature but first decreases up to a certain temperature and then increases to infinity. In contrast, the steady-state value of $I_1(l)$ first rises and then falls down to zero. Details of the temperature behavior of coherent oscillation are different for different loop angles. For instance, for $\theta_{\mathrm{loop}} = 4.5°$ coherent oscillation arises only at $T > 20$ °C. Figures 3 and 4 show the resulting temperature dependence of the normalized stationary intensity $I_1(l)/I_2(l)$ and the onset time $t_{\mathrm{on}}$, respectively. The curves are cut off at temperatures where coherent oscillation disappears. The temperature where the curves reach their maximum ($I_1$-curves) or minimum ($t_{\mathrm{on}}$-curves), as well as the temperature where the oscillation vanishes, increases with increasing $\theta_{\mathrm{loop}}$.

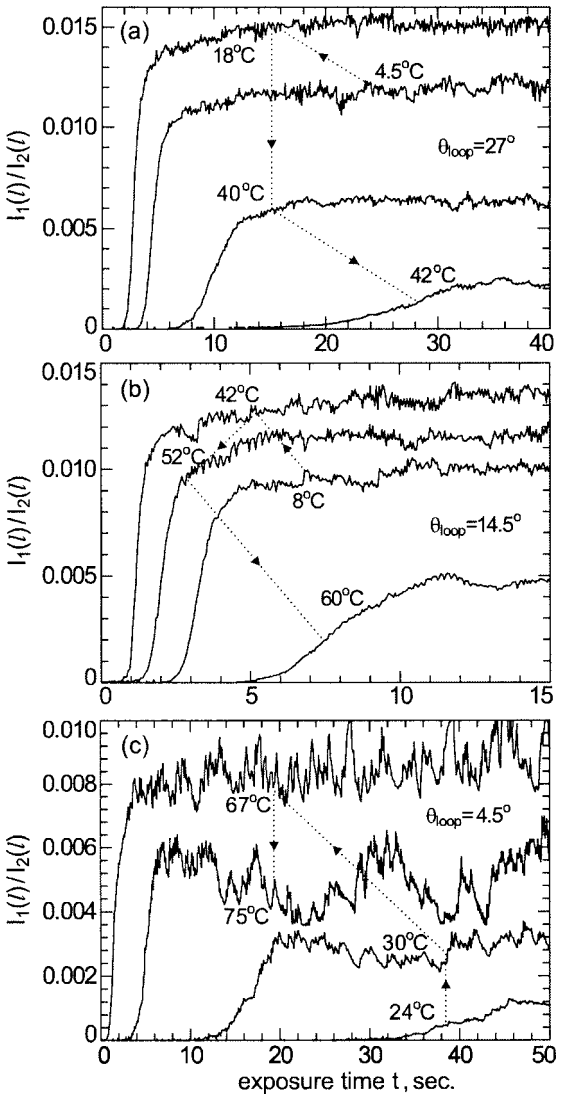


Fig. 2. Dynamics of coherent oscillation at different temperatures in a ring-loop resonator with loop angle $\theta_{loop}$ of (a) 27°, (b) 14.5°, and (c) 4.5°.

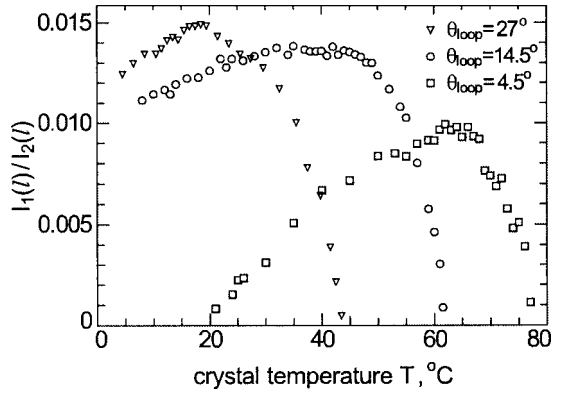


Fig. 3. Normalized intensity of coherent oscillation versus crystal temperature for different angles $\theta_{loop}$: 27°, 14.5°, and 4.5°.

Furthermore, the dynamics of the oscillation decay was measured as follows: After the oscillation signal has reached the steady state, the upper arm of the ring-loop resonator is blocked while the decaying signal is measured via a low-reflection glass plate (not shown in Fig. 1) inserted into the lower arm. The characteristic relaxation time was detected from the tail of the decay kinetics in order to minimize the influence of the Bragg diffraction of the pump beam on the measured signal. The temperature dependence of the decay time $t_{dec}$ is shown in Fig. 5. It strongly decreases with $T$ with no clear extremum, as in the case of $t_{on}$ in Fig. 4.

The influence of the temperature on the oscillation threshold was measured by varying the transmission of the ring-loop cavity. The threshold value of the transmission coefficient $M_{th}$ was very precisely detected by a gradual tuning of the neutral density filter ND. The corresponding results are shown in Fig. 6. The behavior of $M_{th}$ differs for $\theta_{loop}=4.5°$ from that of the other two measuring angles. For the smallest angle, the threshold transmission first decreases with temperature then increases sharply above $T=70$ °C. For all $M_{th}$ curves, the cut-off asymptotes at high temperatures coincide exactly with the ones shown in Figs. 3 and 4.

## 4. DISCUSSION

Since the photorefractive response of SBN depends on ferroelectric properties, it is obvious to suggest that at high $T$ the temperature behavior of coherent oscillation is governed by the gradual decay of the electric polarization $P_s$. At the same time, the broad temperature maximum of

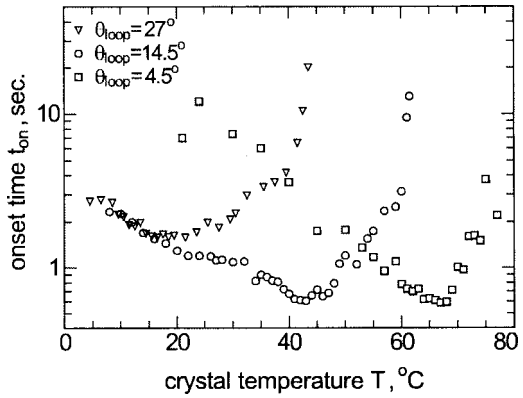


Fig. 4. Oscillation onset time $t_{on}$ versus crystal temperature for different angles $\theta_{loop}$: 27°, 14.5°, and 4.5°.

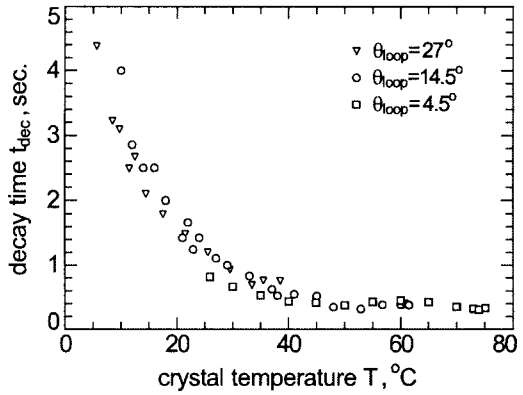


Fig. 5. Oscillation time decay versus crystal temperature for different angles $\theta_{loop}$: 27°, 14.5°, and 4.5°.

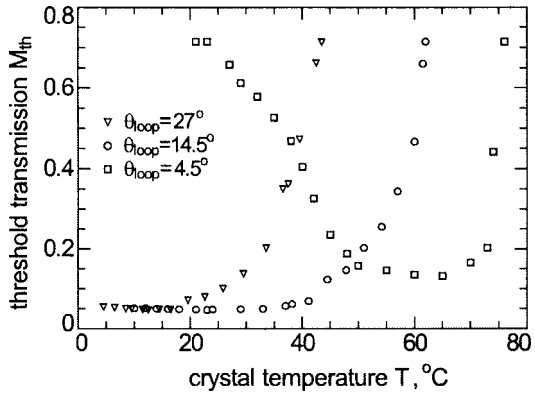


Fig. 6. Threshold transmission coefficient of a ring-loop resonator $M_{\mathrm{th}}$ versus crystal temperature for different angles $\theta_{\mathrm{loop}}$: 27°, 14.5°, and 4.5°.

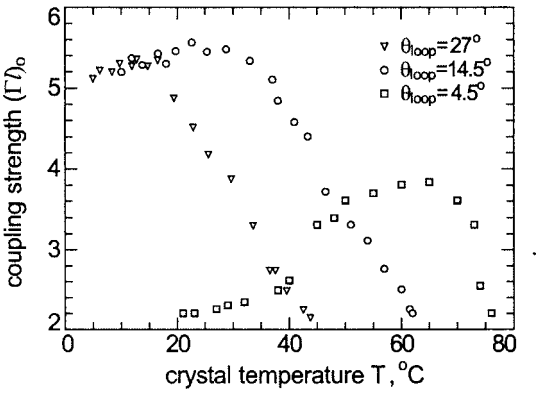


Fig. 7. Stationary coupling strength versus crystal temperature for different angles $\theta_{\mathrm{loop}}$: 27°, 14.5°, and 4.5°.

the electro-optic coefficient $r_{33}$ (Ref. 12) causes an increase of the coupling coefficient $\Gamma_o$ if the crystal is heated below the phase transition. Therefore the initial enhancement of coherent oscillation with increasing $T$ is because of the low-temperature tail of $r_{33}(T)$, whereas the posterior decrease at higher temperatures is caused by a thermal disorder–decay of the polar structure when the crystal is further heated toward the phase-transition temperature and above. This trend results in a maximum of the temperature dependence of both $\Gamma_o$ and $I_1(l)$. Figure 3 verifies this conclusion for the normalized intensity $I_1(l)$. Figure 7 presents the similar temperature dependence of the coupling strength $(\Gamma l)_o$ for the examined angles $\theta_{\mathrm{loop}}$. These dependencies are received by the substitution of the experimental curves $M_{\mathrm{th}}(T)$ in Eq. (2). According to Fig. 7, the oscillation vanishes if the coupling strength $(\Gamma l)_o$ approaches the lowest value of the threshold oscillation $(\Gamma l)_{\mathrm{th}}=2$ calculated for $M=1$ [see Eq. (2)].

An important result of Figs. 3 and 7 is that the temperature of the maximum and of the final decay of the coherent oscillation is different for different loop angles. A similar behavior is observed for the temperature of the minimum of the onset time in Fig. 4. We assume that this difference is a general feature related to relaxor properties of the crystal and particularly is because of the strong dispersion of the thermal disorder–decay processes over different ferroelectric domains. It has already been mentioned that (i) SBN consists of a multitude of domains of different sizes $\Lambda_d$ and (ii) the coupling coefficient $\Gamma_o$ and coherent noise are functions of the temperature-dependent polar structure. Therefore heating results in different changes of coherent oscillation emitted at different angles. An oscillation temperature dependence for the angle $\theta_{\mathrm{loop}}$ is defined by a disorder–decay of domains of the particular size $\Lambda_d$ comparable with the spatial period $\Lambda_g$ of the grating, which solely meets the necessary phase-matching conditions and results in an effective oscillation. Furthermore, just one component of the coherent noise propagating at the angle $\theta_s=\theta_{\mathrm{loop}}$ is attributed to diffraction of the pump beam on scattering structures characterized by $\Lambda_d$. Angles $\theta_{\mathrm{loop}}=4.5°$, 14.5°, and 27° correspond to spatial scales 1, 3, and 6 $\mu$m, respectively. From the positions of the extrema of $I_1(T)$ (Fig. 3) and $t_{\mathrm{on}}(T)$ (Fig. 4), one can estimate the temperature where the thermal energy starts to affect the domain alignment. Here we should note that the strong dependence of the thermal decay on the domain size $\Lambda_d$ is the reason for the remarkable difference between values of the phase-transition temperature detected by different methods.[6] In contrast to the coherent oscillation experiment, the standard methods deal with an averaged response of the crystal integrated over different $\Lambda_d$, and therefore the result strongly depends on the $\Lambda_d$ sensitivity of the particular method.

A comparison of Figs. 3 and 4 shows that the oscillation dynamics are more sensitive to changes in the spatial alignment of ferroelectric domains than the steady-state measurements. The onset time $t_{\mathrm{on}}$ depends on the coupling strength $(\Gamma l)_o$ and on the dielectric relaxation time $\tau_{\mathrm{di}}$. The temperature dependence of $\tau_{\mathrm{di}}$ can be traced to the related dependence of the decay time $t_{\mathrm{dec}}(T)$ shown in Fig. 5, whereas $(\Gamma l)_o$ versus $T$ is shown in Fig. 7. The descending part of $t_{\mathrm{on}}(T)$ has almost the same slope for all three loop angles and is obviously due to the decrease of the dielectric relaxation time $\tau_{\mathrm{di}}$ and the increase of $r_{33}$ below the phase transition. The ascending part is imposed by the thermal disorder–decay that takes place at different temperatures for different $\Lambda_d$. A shift of the extremum of the curve to smaller $T$ with decreasing domain size $\Lambda_d$ (larger $\theta_{\mathrm{loop}}$) is due to the fact that smaller domains are less resistant to the temperature changes. The surprising result of Fig. 4 is the rather low temperature of the extremum found for the largest angle $\theta_{\mathrm{loop}}=27°$. This is possibly because of thermally induced domain fluctuations that become an important factor for small $\Lambda_d$ long before any domain flipping occurs. The thermal fluctuations cause a partial reduction of $P_s$ that then affects $t_{\mathrm{on}}$. The further thermal decay of the polar structure steepens the ascending part of the curve at higher temperatures. The domain resistance to thermal fluctuations increases with $\Lambda_d$, resulting in higher extremum temperatures as well as in the steeper ascending slopes of the dependence $t_{\mathrm{on}}(T)$, (Fig. 4). We assume that the sharpening of the ascending part to a practically vertical line with increasing $\Lambda_d$ corresponds to the approach of the extremum position of the curve to the actual phase-transition temperature of the crystal.

The temperature study of coherent oscillation shows that a heating of the crystal significantly modifies its photorefractive properties. The coupling coefficient $\Gamma_o$ and the

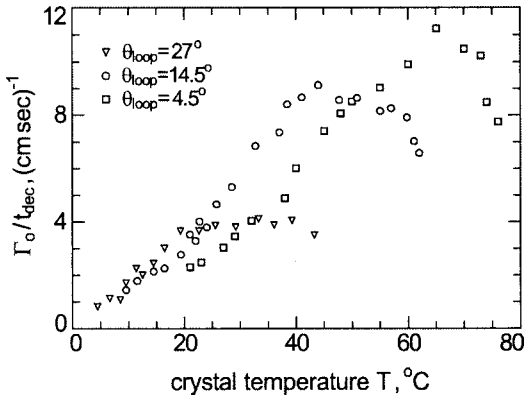


Fig. 8. Ratio $\Gamma_o/t_{\mathrm{dec}}$ versus crystal temperature for different angles $\theta_{\mathrm{loop}}$: 27°, 14.5°, and 4.5°.

dielectric relaxation time $\tau_{\mathrm{di}}$ are the parameters most important for a successful application of the photorefractive material. Therefore an increase of $\Gamma_o$ along with a lowering of $\tau_{\mathrm{di}}$ is a desirable feature that, however, is not always feasible. From Figs. 4 and 7 it can be deduced that the simultaneous effective increase of $\Gamma_o$ and lowering of $\tau_{\mathrm{di}}$ is indeed possible by heating a SBN crystal. The total improvement of these two parameters is illustrated in Fig. 8 by the ratio $\Gamma_o/\tau_{\mathrm{dec}}$ strongly increasing at $T \leqslant T_d$. A tuning range of about 1 order of magnitude is achieved. The values of the coupling coefficient are obtained from Fig. 7, assuming that the interaction length $l$ equals the crystal thickness. At high temperatures, the thermal decay of polar structures results in the limitation of the ratio. Therefore gentle control of the performance of SBN-based photorefractive devices can be easily achieved by changing the temperature of the crystal.

## 5. SUMMARY

In conclusion, the temperature dependence of photorefractive oscillation processes in a ring-loop resonator was studied in SBN:Ce. It has been shown that the coupling strength and the oscillation onset time can be effectively controlled by the temperature of the crystal, and the most noticeable improvement occurs when approaching the phase transition. The temperature behavior of coherent oscillation is explained as a result of the strong dependence of the photorefractive response on the relaxor properties of SBN. The temperature impact on the polar structure decay is found to be different for ferroelectric domains of different sizes $\Lambda_d$.

The work is supported by INTAS (01-0173), DFG (IM 37/2-1, WO618/3-4, GRK 695).

## REFERENCES

1. P. Yeh, *Introduction to Photorefractive Nonlinear Optics* (Wiley, 1993).
2. M. Cronin-Golomb, B. Fisher, J. P. White, and A. Yariv, "Theory and applications of four-wave mixing in photorefractive media," IEEE J. Quantum Electron. **20**, 12–30 (1984).
3. S. Odoulov, M. Soskin, and A. Khizhnyak, *Introduction to Photorefractive Nonlinear Optics* (Harwood, 1998).
4. M. Goulkov, M. Imlau, R. Pankrath, T. Granzow, U. Dörfler, and Th. Woike, "Temperature study of photo-induced wide-angle scattering in cerium-doped strontium barium niobate," J. Opt. Soc. Am. B **20**, 307–313 (2003).
5. M. Goulkov, T. Granzow, U. Dörfler, Th. Woike, M. Imlau, and R. Pankrath, "Study of beam-fanning hysteresis in photorefractive SBN:Ce: light-induced and primary scattering as functions of polar structure," Appl. Phys. B **76**, 407–416 (2003).
6. M. Goulkov, O. Shinkarenko, T. Granzow, Th. Woike, and M. Imlau, "Beam fanning used to study thermal disorder and decay of polar structures in the ferroelectric relaxor $Sr_{0.61}Ba_{0.39}Nb_2O_6$," Europhys. Lett. **66**, 48–54 (2004).
7. M. Goul'kov, S. Odoulov, and R. Troth, "Temporal threshold of oscillation in ring-loop photorefractive resonator," Ukr. J. Phys. **36**, 1007–1009 (1991).
8. M. Cronin-Golomb, A. M. Biernacki, C. Lin, and H. Kong, "Photorefractive time differentiation of coherent optical images," Opt. Lett. **12**, 1029–1031 (1987).
9. A. J. Fox, "Longitudinal electro-optic effects in barium strontium niobate ($Sr_{1-x}Ba_xNb_2O_6$)," J. Appl. Phys. **44**, 254–262 (1973).
10. G. Fogarty, B. Steiner, M. Cronin-Golomb, U. Laor, M. H. Garrett, J. Martin, and R. Uhrin, "Antiparallel ferroelectric domains in photorefractive barium titanate and strontium barium niobate observed by high-resolution x-ray diffraction imaging," J. Opt. Soc. Am. B **13**, 2636–2643 (1996).
11. L. Ivleva, N. Bogodaev, N. Polozkov, and V. Osiko, "Growth of SBN single crystals by Stepanov technique for photorefractive applications," Opt. Mater. **4**, 168–173 (1995).
12. M. Goulkov, T. Granzow, U. Dörfler, Th. Woike, M. Imlau, and R. Pankrath, "Temperature dependent determination of the linear electrooptic coefficient $r_{33}$ in $Sr_{0.61}Ba_{0.39}Nb_2O_6$ single crystals by means of light-induced scattering," Opt. Commun. **218**, 173–182 (2003).